IOP Publishing Measurement Science and Technology
Meas. Sci. Technol. **31** (2020) 055203 (11pp) https://doi.org/10.1088/1361-6501/ab63b0

Efficient method for detecting a zero-phase point in off-axis circular fringe projection profilometry

Chunwei Zhang[1,2], Hong Zhao[1,3], Zhenyang Zhang[1], Jiacheng Qiao[1], Jinlei Zhao[1,4], Changquan Zhou[5] and Juntong Xi[2,6]

[1] School of Mechanical Engineering, Xi'an Jiaotong University, No. 28 Xianning West Road, Xi'an, Shaanxi 710049, People's Republic of China
[2] State Key Laboratory for Mechanical System and Vibration, No. 800 Dongchuan Road, Shanghai 200240, People's Republic of China
[3] State Key Laboratory for Manufacturing Systems Engineering, No. 99 Yanxiang Road, Xi'an, Shaanxi 710054, People's Republic of China
[4] No. 203 Research Institute of China Ordnance Industries, No. 10 Zhangba East Road, Xi'an, Shaanxi 710065, People's Republic of China
[5] Luoyang Institute of Electro-Optical Devices, No. 25 Kaixuan West Road, Luoyang, Henan 471000, People's Republic of China
[6] School of Mechanical Engineering, Shanghai Jiao Tong University, No. 800 Dongchuan Road, Shanghai 200240, People's Republic of China

E-mail: zcw198811@163.com and zhaohong@mail.xjtu.edu.cn

Received 6 September 2019, revised 4 December 2019
Accepted for publication 18 December 2019
Published 26 February 2020

Abstract

Off-axis circular fringe projection profilometry (OCFPP) is a kind of recently proposed three-dimensional (3D) measurement technique. Coordinates of the zero-phase point is an indispensable parameter for the application of OCFPP. As the zero-phase point is virtual, calculation of its coordinates is a key problem to be solved. To efficiently and accurately calculate the coordinates of the zero-phase point, a compound method is put forward in this paper. Firstly, a method is proposed to detect the coarse coordinates of the zero-phase point with the aid of the property of the phase distribution; then, a fast searching strategy is presented to efficiently detect the exact coordinates. The coarse coordinates provide a reasonable center for the following fast searching. The foundation of the fast searching strategy is laid with the aid of a constructed mathematical model and computer simulation. Benefits of the compound method are twofold: firstly, it makes it possible to locate the searching center without usage of an additional ruler; secondly, it significantly improves the efficiency of detecting the zero-phase point while keeping the accuracy. Experiments confirm the advantages of the proposed method.

Keywords: off-axis, zero-phase point detection, three-dimensional measurement, circular fringe projection profilometry

(Some figures may appear in colour only in the online journal)

1. Introduction

Fringe projection profilometry (FPP) is being employed for three-dimensional (3D) measurement more and more widely [1–9]. Since FPP was proposed [10], more than 35 years have passed. The fundamental problems concerning FPP, such as phase demodulation [10–13], phase unwrapping [14–18], and system calibration [19–25], have been well studied. At present, more attention is being paid to improving the measurement performance of FPP under variant practical measurement

conditions. Raising the measurement accuracy is among the key objectives. In order to raise the accuracy, an effective measure is to equip a camera or a projector with telecentric lenses [26–34]. The reason is manifest: the usage of telecentric lenses can evidently improve the transverse resolution, which will eventually contribute to raising the measurement accuracy in the height.

Circular fringe projection profilometry (CFPP) is a special kind of FPP with telecentric lenses [35–37]. The specialty lies in that CFPP recovers the 3D profile based on the triangulation formed between the optical axis and the projected light rays of a projector. Accordingly, the hardware layout, the coded fringe pattern and the 3D reconstruction model differ with those of FPP. CFPP is proposed to explore a novel 3D measurement technique, and is expected to outperform the performance of FPP in terms of measurement accuracy. However, the performance of CFPP remains to be further developed.

When the zero-phase point is located within the field of view of a CFPP system, the intersection angles between the projection lights and the optical axis approximate to zero at the region near the optical axis. Then, errors in the measured parameters at the region will be dramatically amplified because values of cotangent of the intersection angles are extremely large. This will bring in tremendous error to the recovered 3D profile. To deal with this problem, off-axis CFPP (OCFPP) is recently presented [37]. In OCFPP, the axes of a camera and a projector are adjusted to be far away. OCFPP helps to improve the 3D measurement accuracy. However, it also brings in an accessional issue that the zero-phase point stands outside the field of view of the camera. This means that its pixel coordinate, which is indispensable for 3D reconstruction, is lost. In [37], two methods, called the two-dimensional (2D) ruler-based method (2DRM) and the plane constraint-based method (PCM) are respectively presented to solve this problem. These methods are far from enough because the 2DRM can only ensure a coarse result with the aid of a 2D ruler while the PCM can obtain a fine result at the expense of huge time consumption. Furthermore, the application of the PCM requires that a reasonable searching center be provided in advance. To obtain the searching center, a method such as the 2DRM has to be adopted beforehand. In practice, it is expected that the zero-phase point could be accurately calculated with high efficiency and without relying on an additional 2D ruler.

This paper solves this problem by proposing a novel compound method to efficiently and accurately detect the zero-phase point. The proposed method is composed of two connected methods. The first method is called the circle fitting-based method (CFM) for simplicity. The CFM is used to work out the coarse coordinates of the zero-phase points by applying circle fitting to phases of a captured circular fringe pattern. The second method is called the recursive plane constraint-based method (RPCM) for simplicity. The coarse coordinates obtained with the CFM will be used as the first-round searching center of the RPCM. RPCM is capable of searching for the accurate coordinates in an efficient way since a fast searching strategy similar to the binary search strategy is adopted. To ensure that the efficient searching strategy is tenable, mathematical deviation and computer simulation are conducted.

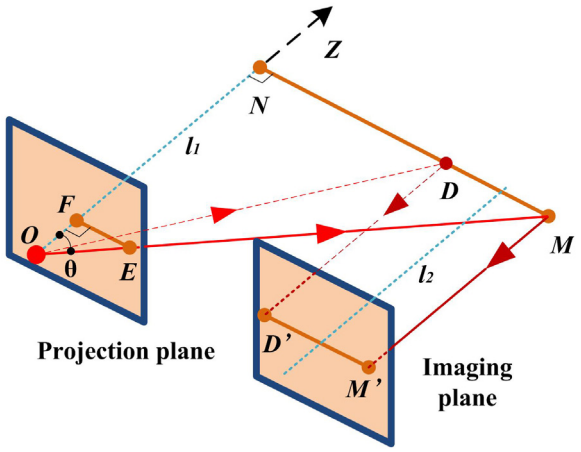

Figure 1. Geometry of OCFPP.

The CFM, in combination with the RPCM, will be called the circle-fitting RPCM (CRPCM) for simplicity. The CRPCM contributes to evidently improving the efficiency to detect the zero-phase point while saving the usage of an auxiliary 2D ruler. Consequently, it helps to further enhance the performance of OCFPP.

The rest of this paper is structured as follows: in section 2, OCFPP is briefly introduced, and the origin of the problem of detecting the zero-phase point is explained; in section 3, theoretical foundation of CFM and RPCM is proven, CFM and RPCM are described, and procedures for CRPCM are outlined; in section 4, experiments are performed to check the practical performance of CRPCM, and discussions are made; in section 5, this paper is summarized.

2. Off-axis circular fringe projection profilometry (OCFPP)

2.1. Brief introduction to OCFPP

It is recommended that [35–37] be referred to in advance because this paper builds on theories therein.

Similar to FPP, OCFPP is also a triangulation-based 3D measurement technique. The triangle it relies on is depicted in figure 1. ON is perpendicular to the projection plane, M denotes any point on a measured surface, $MN \perp ON$, the angle between OM and ON is θ, and $MN//EF$. Lines l_1 and l_2 represent the optical axes of the adopted projector and camera respectively, and $l_1//l_2$. The core of OCFPP is to calculate the z coordinate of the point M (i.e. the length of ON) with the aid of MN and θ. ΔOMN and the projection plane constitute a model like a reverse pinhole model, which can be readily realized by a projector. However, direct calculation of MN and θ are impossible since the point N is virtual in practice. To this end, a kind of circular fringe pattern, a conventional projector and a camera equipped with telecentric lenses are used. Then, θ can be signified by the phase of the circular fringe pattern and intrinsic parameters of the projector; MN can be signified by the phase of the circular fringe pattern, the image coordinate of the zero-phase point, and intrinsic parameters of the camera and telecentric lenses. It can be worked out that the 3D reconstruction model of OCFPP can be expressed as [35–37]

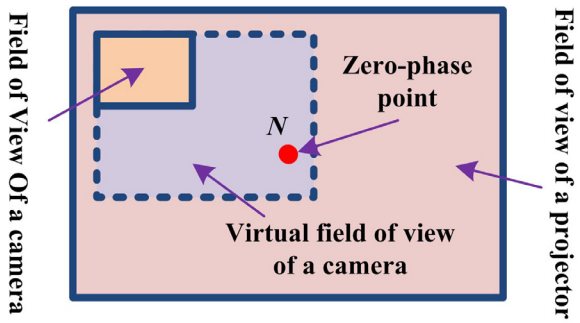

Figure 2. Schematic diagram of field of views of a camera and a projector in OCFPP.

$$\begin{cases} x(x_c, y_c) = \mu_c x_c/\beta + \xi_x \\ y(x_c, y_c) = \mu_c y_c/\beta + \xi_y \\ z(x_c, y_c) = (\mu_c \sqrt{(x_c - x_{c0})^2 + (y_c - y_{c0})^2})/(k\beta\Phi(x_c, y_c)) \end{cases}, \tag{1}$$

where μ_c denotes the physical size of pixels of a used digital camera, (x_c, y_c) are pixel coordinates of any point in captured images, β represents the amplification factor of the employed telecentric lenses, ξ_x and ξ_y are constants only determined by the origin of the world coordinate system, (x_{c0}, y_{c0}) represents pixel coordinates of the zero-phase point in a captured circular fringe pattern, $\Phi(x_c, y_c)$ is the phase of the captured circular fringe pattern, and k is a parameter determined by intrinsic parameters of the projector and the period of the coded circular fringe pattern.

Errors always exist in values of all parameters in the 3D reconstruction model. From equation (1), it can be inferred that when $\Phi(x_c, y_c)$ approximates to zero, the calculated value of z will be severely distorted by the potential error. It has been theoretically demonstrated that the larger the value of θ, the better the measurement accuracy for OCFPP will become on the condition that θ is less than a threshold around 0.7 radians [37]. The maximum divergence angle of a conventional projector is generally less than 0.7 radians. Hence, the distance between l_1 and l_2 should be set as large as possible to improve the measurement accuracy.

2.2. Zero-phase point problem in OCFPP

The departure of l_1 and l_2 helps to enhance the measurement performance of OCFPP. In practice, the distance between l_1 and l_2 should be adjusted to be so large that the point N in figure 1 is always out of the field of view of the imaging system. This phenomenon is further exhibited in figure 2. It can be seen that the field of views of the camera and the projector are very different in OCFPP. The reason is that the camera is equipped with telecentric lenses while the projector has conventional lenses. The point N in figure 2 is the same as the one in figure 1. It is the zero-phase point. The phase of a projected circular fringe pattern is always zero at this point (it makes up a line coinciding with l_1 in figure 1). If the zero-phase point could be imaged, its coordinates would be (x_{c0}, y_{c0}). However, as can be seen from figure 2, the point N cannot be imaged by the camera in OCFPP. Accordingly, it becomes impossible to detect (x_{c0}, y_{c0}) by searching for the point whose phase value is zero in the phase map of an acquired circular fringe pattern. (x_{c0}, y_{c0}) become lost in OCFPP. This prevents the application of equation (1), and makes it impossible to accomplish the 3D measurement with OCFPP. Measures have to be taken to solve this problem.

2.3. Shortcomings in the PCM

In [37], the PCM is put forward to detect the zero-phase point. It will be briefly introduced here because the method in this paper is partly built on the PCM.

Considering that μ_c, k and β all are constants, and their values are set to 1, the equation for calculating the z coordinate (please refer to equation (1)) becomes

$$z_{\text{virtual}}(x_c, y_c) = \frac{\sqrt{(x_c - x_{c0})^2 + (y_c - y_{c0})^2}}{\Phi(x_c, y_c)}. \tag{2}$$

Obviously,

$$z_{\text{virtual}}(x_c, y_c) = \lambda z(x_c, y_c), \tag{3}$$

where λ is constant.

From equation (3), it can be inferred that the shape of $z_{\text{virtual}}(x_c, y_c)$ is the same to that of $z(x_c, y_c)$. Therefore, if a flat board is measured with OCFPP, the virtual profile recovered with the aid of equation (2) should be a plane. The problem lies in that (x_{c0}, y_{c0}) are unknown. The planeness of the recovered profile is best only when (x_{c0}, y_{c0}) takes its actual value. As presented in [37], this property can be utilized to detect (x_{c0}, y_{c0}). Suppose a flat board is measured with OCFPP, q is any point within a region covering the actual zero-phase point, and its coordinates are (x^q_{c0}, y^q_{c0}). Accordingly,

$$z^q_{\text{virtual}}(x_c, y_c) = \frac{\sqrt{(x_c - x^q_{c0})^2 + (y_c - y^q_{c0})^2}}{\Phi(x_c, y_c)}. \tag{4}$$

Then plane fitting is applied to $z^q_{\text{virtual}}(x_c, y_c)$, and the obtained plane is signified by $z^q_{fit}(x_c, y_c)$. The root mean square error (RMSE) of the plane fitting can be calculated by

$$\text{RMSE}(q) = \sqrt{\frac{\sum_{x_c=1}^{\text{column}} \sum_{y_c=1}^{\text{row}} (z^q_{virtual}(x_c, y_c) - z^q_{fit}(x_c, y_c))^2}{row \cdot column}}, \tag{5}$$

where *row* and *column* denote the total row number and column number of the captured image respectively.

Now that the measured object is a flat board, it is obvious that the following relationship stands:

$$(x_{c0}, y_{c0}) = (x^{\bar{q}}_{c0}, y^{\bar{q}}_{c0}), \tag{6}$$

where

$$\bar{q} = \min_{q=1,2,\cdots} \text{RMSE}(q). \tag{7}$$

The above-mentioned method is the PCM proposed in [37]. Its searching process is explained in figure 3. The total number of points to be searched is

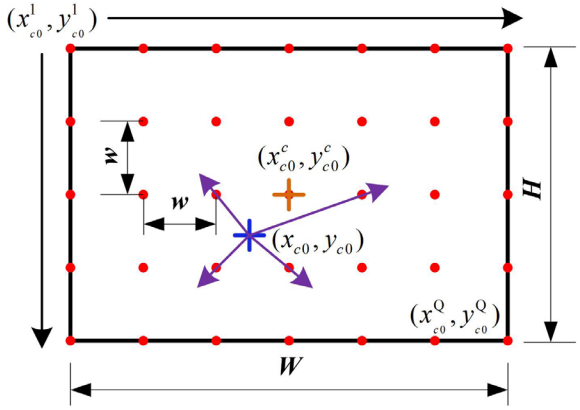

Figure 3. Explanation to the searching process of the PCM: (x^c_{c0}, y^c_{c0}) denotes the center of the selected searching region, (x_{c0}, y_{c0}) denotes the actual zero-phase point, (x^1_{c0}, y^1_{c0}) denotes the first searching point, (x^Q_{c0}, y^Q_{c0}) denotes the last searching point, the window size is $W \times H$, the searching width is w, and the purple arrows signify the radial directions.

$$Q = \frac{W}{w} \cdot \frac{H}{w}. \tag{8}$$

In order to accurately detect the zero-phase point, the step width w should be set to a small value. In order to ensure the searching region covers the actual zero-phase point, W and H should be set relatively large. Suppose $W = H = 500$ and $w = 0.1$ (this is not a harsh condition in practice), it can be computed that totally 25 000 000 points should be searched, which means 25 000 000 times plane fitting have to be implemented. This is too time-consuming. Furthermore, the searching center should be obtained before the PCM is employed. At present, this can be accomplished with the aid of the 2DRM, which is also proposed in [37]. However, the application of the 2DRM requires a 2D ruler be used, which makes the actual operation complex. An efficient and handy method for detecting the zero-phase point in OCFPP remains to be investigated.

3. Principle of the circle-fitting recursive plane constraint-based method (CRPCM)

The CRPCM is proposed to accurately and efficiently detect the zero-phase point for OCFPP. It realizes this goal by two core steps: firstly, it calculates the coarse location of the zero-phase point by implementing circle fitting to the absolute phase of a circular fringe pattern captured from a flat board; then, a recursive PCM is applied to search for the zero-phase point with both accuracy and efficiency. This will be concretely described in the following.

3.1. Circle fitting method (CFM) for detecting the coarse zero-phase point

The phase of a coded circular fringe pattern is regular. It is proportional to the distance between any point and the zero-phase point, which can be expressed as [35]

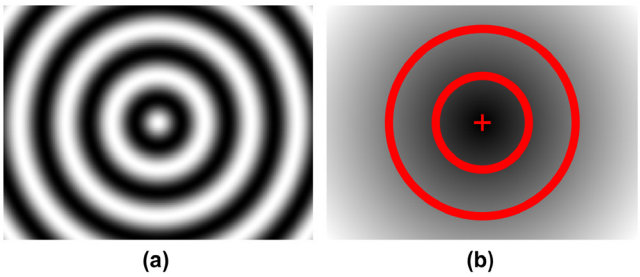

Figure 4. (a) A coded circular fringe pattern and (b) its phase: the size of the image is 300 × 400 (row × column), $R_p = 60$, $(x_{p0}, y_{p0}) = (200.5, 150.5)$, and red circles in the right image mark pixels with values of 2π (inner) and 4π (outer) respectively.

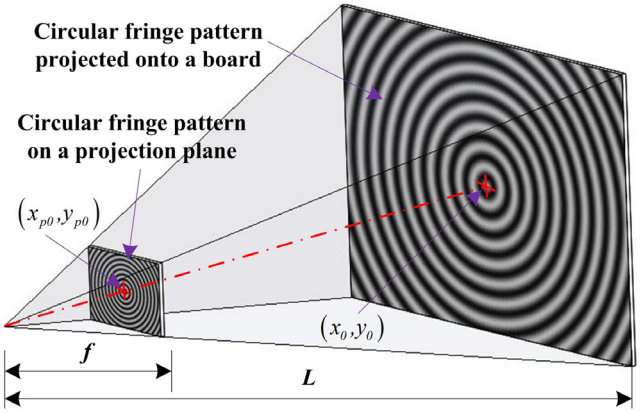

Figure 5. A coded circular fringe pattern projected onto a flat board, which is perpendicular to the optical axis of the employed projector.

$$\Phi(x_p, y_p) = 2\pi \frac{\sqrt{(x_p - x_{p0})^2 + (y_p - y_{p0})^2}}{R_p}, \tag{9}$$

where $\Phi(x_p, y_p)$ denotes the phase at point (x_p, y_p), (x_{p0}, y_{p0}) are coordinates of the zero-phase point, and R_p represents the fringe period in the pixel of the coded circular fringe pattern.

Note that (x_{p0}, y_{p0}) should be the pixel coordinates of the point F in figure 1 ideally. From equation (9), it can be inferred that pixels with the same phases form a set of concentric circles with the center being (x_{p0}, y_{p0}). This phenomenon is visualized in figure 4. Therefore, if the phases of a subregion of the coded circular fringe pattern are known, the coordinates of its zero-phase point, (x_{p0}, y_{p0}), can be calculated by performing circle fitting to any set of points with the same phase value.

When a circular fringe pattern, as shown in figure 4(a), is projected onto a flat board that is perpendicular to the optical axis of the projector, its spatial distribution will be amplified with a ratio determined by focal length of the projector and distance between the optical center of the projector and the flat board (see figure 5). Accordingly, the phase distribution on the flat board becomes

$$\Phi(x, y) = 2\pi \frac{\sqrt{(x - x_0)^2 + (y - y_0)^2}}{R}, \tag{10}$$

where (x, y) and (x_0, y_0) can be regarded as coordinates in millimeters of any point and the zero-phase point in the world

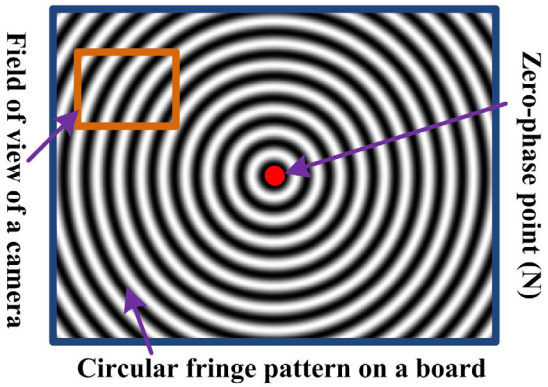

Figure 6. Circular fringe pattern on a flat board and the region actually captured by a camera with telecentric lenses: the orange solid rectangle marks the captured circular fringe pattern.

coordinate system respectively, $\Phi(x, y)$ is the phase of the circular fringe pattern at point (x, y), and

$$\begin{cases} x = \alpha u_p x_p \\ y = \alpha u_p y_p \\ R = \alpha u_p R_p \end{cases}, \tag{11}$$

where μ_p denotes the physical size of pixels of a used digital projector, and $\alpha = L/f$.

From equation (10), it can be inferred that points with the same phase values on the flat board form a set of concentric circles centering at (x_0, y_0). Hence, if the phases of a subregion of the circular fringe pattern on the flat board are known, the coordinates of its zero-phase point, (x_0, y_0), can be calculated by performing circle fitting to any set of points with the same phase value.

The circular fringe pattern on the flat board will be captured by a camera with telecentric lenses. As shown in figure 1, the optical axis of the camera is parallel to that of the projector. According to the imaging law of telecentric lenses, the circular fringe pattern keeps to the circular fringe pattern when imaged by the camera. Figure 6 exemplifies this phenomenon. The orange solid rectangle signifies the actual field of view of the camera with telecentric lenses. As can be seen, only a small part of circular fringe pattern on the flat board can be seen by the camera. It can be inferred that phases of circular fringe pattern captured by the camera obey the following equation:

$$\Phi(x_c, y_c) = 2\pi \frac{\sqrt{(x_c - x_{c0})^2 + (y_c - y_{c0})^2}}{R_c}, \tag{12}$$

where

$$R_c = \frac{\beta R}{\mu_c}. \tag{13}$$

Hence, it can be inferred that coordinates of the virtual zero-phase point, (x_{c0}, y_{c0}), can be calculated with the aid of circle fitting theoretically.

In practice, it is difficult to set a board to be strictly perpendicular to the optical axis of a projector, and other kinds of error in the calculated parameters are also unavoidable. These factors make the accuracy of (x_{c0}, y_{c0}) obtained by circle fitting not high. However, it provides a convincing searching center required for detecting the exact zero-phase point. Note that both the flat board and the circular fringe patterns required in CFM can be obtained in the conventional calibration process of the OCFPP system. Hence, the application of the CFM consumes little resources.

3.2. RPCM for detecting the exact zero-phase point

Suppose the coarse coordinates calculated with the CFM is (x^c_{c0}, y^c_{c0}), a searching window centered at (x^c_{c0}, y^c_{c0}) with a size of $W \times H$ being selected, as shown in figure 3. As noted in section 2.3, it will be too time-consuming if the selected region is searched point by point with a constant searching step, i.e. w remaining constant. It is easy to think of employing a fast searching strategy instead of the exhaustive search. However, does the feasibility of a fast searching strategy stand?

3.2.1. Demonstration of the feasibility of a fast searching strategy. If the distribution of the planeness of recovered virtual profiles are inversely proportional to the distance between any point and the zero-phase point along the radial direction (please refer to figure 3), then a binary search can be employed to efficiently detect the zero phase point. Does this assumption stand? This will be answered by mathematical deviation and computer simulation.

When a flat board is measured with OCFPP, and suppose its height distribution, $z(x_c, y_c)$, is known in advance, according to equation (1), the phase distribution of the captured circular fringe pattern can be expressed as

$$\Phi(x_c, y_c) = \frac{\mu_c \sqrt{(x_c - x_{c0})^2 + (y_c - y_{c0})^2}}{k\beta z(x_c, y_c)}. \tag{14}$$

Combining equation (4) with (14), it can be worked out that

$$z^q_{\text{virtual}}(x_c, y_c) = z(x_c, y_c) f_q(x_c, y_c), \tag{15}$$

where

$$f_q(x_c, y_c) = \sqrt{\frac{(x_c - x^q_{c0})^2 + (y_c - y^q_{c0})^2}{(x_c - x_{c0})^2 + (y_c - y_{c0})^2}}. \tag{16}$$

Note that μ_c, k, and β are all set to be 1 for clarity because this does not impact the planeness of $z^q_{\text{virtual}}(x_c, y_c)$. Now that the measured object is a flat board, $z(x_c, y_c)$ should represent a plane. Similarly, $z^q_{\text{virtual}}(x_c, y_c)$ represents a plane if and only if $(x^q_{c0}, y^q_{c0}) = (x_{c0}, y_{c0})$. At this time, $f_q(x_c, y_c) = 1$, and hence $z^q_{\text{virtual}}(x_c, y_c) = z(x_c, y_c)$. This coincides with the conclusion in section 2.3 that the planeness of the recovered virtual profile of a measured flat board is best only when $(x^q_{c0}, y^q_{c0}) = (x_{c0}, y_{c0})$. What is interested in is whether or not the planeness of profiles recovered at each searched point, (x^q_{c0}, y^q_{c0}), is inversely proportional to the distance between the point and the actual zero-phase point along the radial direction. This is a complex mathematical proof problem for one who does not major in mathematics. However, it can be proven by mathematical modeling and computer simulation.

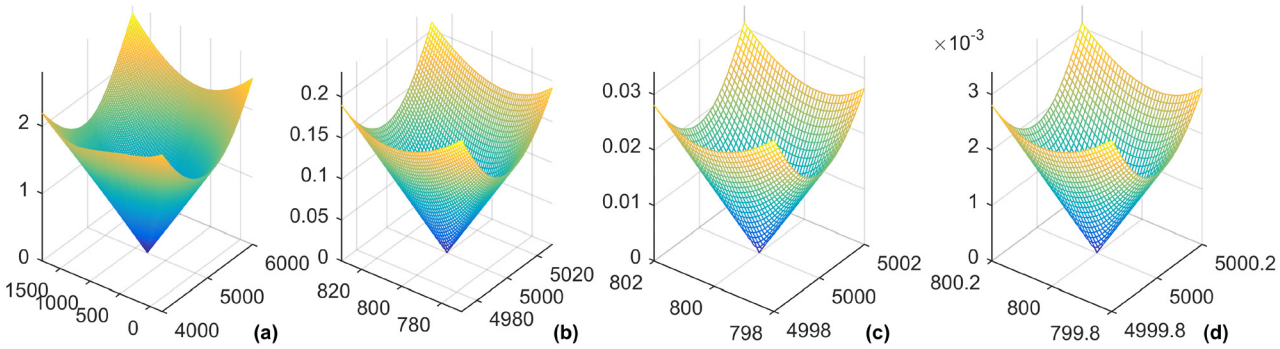

Figure 7. Distributions of *curvature*(q): (a) $W_1 \times H_1 = (2000, 2000)$, and $w_1 = 20$; (b) $W_2 \times H_2 = (60, 60)$, and $w_2 = 1$; (c) $W_3 \times H_3 = (4, 4)$, and $w_3 = 0.1$; (d) $W_4 \times H_4 = (0.4, 0.4)$, and $w_4 = 0.01$.

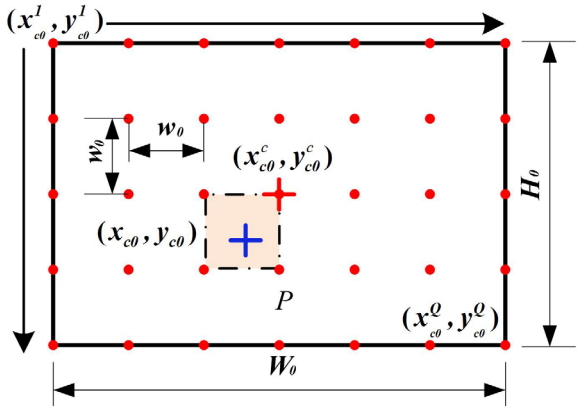

Figure 8. The region (the orange region) that covers the actual zero-phase point detected by first-round searching: the planeness of four vertexes of the orange region are better than that of other points, the blue cross whose coordinates are (x_{c0}, y_{c0}) marks the actual zero-phase point, the red cross whose coordinates are (x_{c0}^c, y_{c0}^c) marks the center of the selected first-round searching window, the first-round window size is $W_0 \times H_0$, and the first-round searching step is w_0.

When $(x_{c0}^q, y_{c0}^q) \neq (x_{c0}, y_{c0})$, the profile of $f_q(x_c, y_c)$ will deviate from $f_q(x_c, y_c) = 1$ disproportionally, and hence the profile of $z_{\text{virtual}}^q(x_c, y_c)$ will become curved (please refer to equation (15)). Considering that $z(x_c, y_c)$ denotes a plane, the curvature of $z_{\text{virtual}}^q(x_c, y_c)$ is resulted from $f_q(x_c, y_c)$. Concretely, the larger the deviation of $f_q(x_c, y_c)$ from a horizontal plane, the larger the curvature of $z_{\text{virtual}}^q(x_c, y_c)$ will become. Therefore, the curvature of $z_{\text{virtual}}^q(x_c, y_c)$ can be quantified by

$$curvature(q) = \frac{\sum_{x_c=1}^{\text{column}} \sum_{y_c=1}^{\text{row}} \left| f_q(x_c, y_c) - \bar{f}(q) \right|}{row \times column}, \quad (17)$$

where $\bar{f}(q)$ represents a horizontal plane determined by $f_q(x_c, y_c)$:

$$\bar{f}(q) = \frac{\sum_{x_c=1}^{\text{column}} \sum_{y_c=1}^{\text{row}} f_q(x_c, y_c)}{row \times column}. \quad (18)$$

Hence, the above-mentioned problem is transformed to whether or not there is one and only one local minimum value for *curvature*(q). This problem can be solved with the aid of computer simulation. If the distribution of *curvature*(q) along with (x_{c0}^q, y_{c0}^q) had one and only one local minimum value that locates at (x_{c0}, y_{c0}) under representative simulated conditions, the above-mentioned problem can be proven.

Suppose $(x_{c0}, y_{c0}) = (5000, 800)$, *curvature*$(q)$ with $W_1 \times H_1 = (2000, 2000)$ (please refer to figure 3), $w_1 = 20$; $W_2 \times H_2 = (60, 60)$, $w_2 = 1$; $W_3 \times H_3 = (4, 4)$, $w_3 = 0.1$; $W_4 \times H_4 = (0.4, 0.4)$, $w_4 = 0.01$ are considered respectively. Figure 7 depicts the calculated *curvature*(q). The searched region is gradually subdivided to detect all of the potential local minimum values besides (x_{c0}, y_{c0}). It is clear that all minimum values of *curvature*(q) are unique, and locate at $(5000, 800)$. Hence, it can be safely concluded that the local minimum value of *curvature*(q) is unique. This lays the foundation for the adoption of a fast searching strategy.

3.2.2. Recursive plane constraint-based method (RPCM). Now that there is one and only one minimum value for *curvature*(q) that locates at the actual zero-phase point (see figure 7), and a fast searching strategy becomes available. Once $\Phi(x_c, y_c)$, $z_{\text{virtual}}^q(x_c, y_c)$ and (x_{c0}^c, y_{c0}^c) are calculated, the location of the zero-phase point can be searched as follows (see figure 8):

Step 1: set the first-round searching step to be w_0, the size of first-round searching window centered at (x_{c0}^c, y_{c0}^c) to be $W_0 \times H_0$ (values of W_0 and H_0 should be relatively large, such as 1024), and calculate all of the values of $z_{\text{virtual}}^q(x_c, y_c)$ with the aid of equation (4).

Step 2: the four points that make the planeness of $z_{\text{virtual}}^q(x_c, y_c)$ better than that of the other points are detected, and they make up a region to be searched in the next round.

Step 3: procedures similar to steps 1 and 2 are recursively applied until $w_i \leqslant thr_{\text{set}}$, thr_{set} should be a small value, such as 0.01, and during the recursive searching process, the searching step and the size of the searching window could be set to

$$\begin{cases} w_j = w_{j-1}/\varepsilon \\ W_j \times H_j = w_{j-1} \times w_{j-1} \end{cases}, j = 1, 2, \ldots J, \quad (19)$$

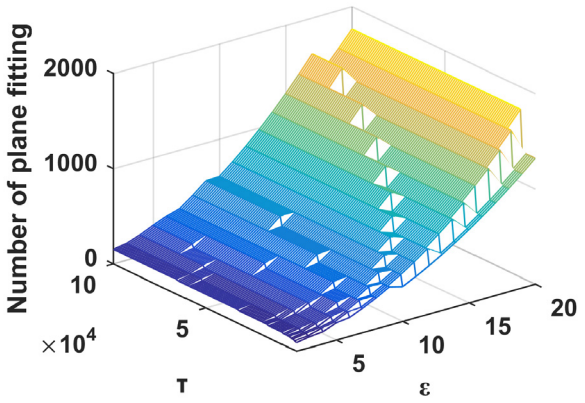

Figure 9. Distribution of the required number of plane fitting along with ε and τ.

where ε is an integer larger than 1, J is a number that makes $w_J \leqslant thr_{\text{set}}$.

Step 4: coordinates of the zero-phase point is the one making the planeness of $z^q_{\text{virtual}}(x_c, y_c)$ best in the last-round searching.

The above searching process is called the RPCM for simplicity.

There are many strategies that can be adopted to select w_0. A preferred one is as follows:

$$w_0 = \begin{cases} W/\varepsilon, & \text{if } W \geqslant H \\ H/\varepsilon, & \text{if } W < H \end{cases}. \tag{20}$$

Then, the total number of plane fitting during the application of the RPCM can be calculated by (assume $W = H$ for simplicity):

$$f(\varepsilon, \tau) = (\varepsilon + 1)^2 \text{ceil}(\log_\varepsilon \tau), \tag{21}$$

where $\text{ceil}(*)$ means taking the smallest integer that is no less than $*$, and $\tau = W/thr_{\text{set}}$.

Distribution of $f(\varepsilon, \tau)$ when $\varepsilon \in [2, 20]$ and $\tau \in [10^3, 10^5]$ is plotted in figure 9. It is clear that $\varepsilon = 2$ should be chosen to ensure the best efficiency. When $\varepsilon = 2$, and assume $W = H$, the ratio between the number of plane fitting required by the PCM and that by the RPCM is

$$R(\tau) = \frac{(\tau + 1)^2}{9\text{ceil}(\log_2 \tau)}. \tag{22}$$

Figure 10 depicts the distribution of equation (22). The value of τ is seldom smaller than 1000 in practice. Therefore, it can be found that the efficiency of the RPCM should be more than 10 000 times faster than that of the PCM.

3.3. Procedures of CRPCM

The CRPCM is a combination of the CFM and RPCM. Its working principle is as follows:

Step 1: a flat board is placed within the field of view of an OCFPP system, and it is adjusted to be as perpendicular to the axis of a projector in the OCFPP system as possible.

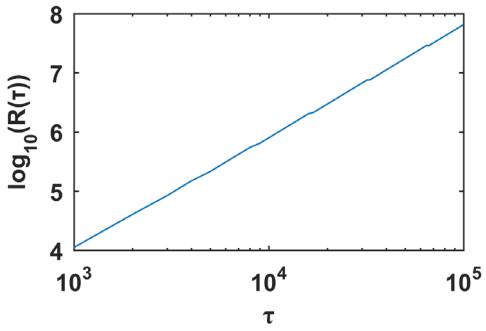

Figure 10. Ratio between the efficiency of the RPCM and PCM when $\varepsilon = 2$.

Step 2: a set of circular fringe patterns are projected onto the flat board, and they are imaged.

Step 3: $\Phi(x_c, y_c)$ is calculated from the acquired circular fringe patterns.

Step 4: CFM is applied to detect the coarse coordinates of the zero-phase point, i.e. (x^c_{c0}, y^c_{c0}) which will be used as the first-round searching center of RPCM.

Step 5: RPCM is applied to detect the actual coordinates of the zero-phase point.

The perpendicularity in step 1 is just to obtain a more accurate searching center with the CFM. It is not required by the RPCM. The application of the CRPCM can be realized with little resource consumption because the required flat board and phase can be provided by the conventional system calibration process.

4. Experiments and discussions

Experiments were conducted to validate the CRPCM. In the experiments, the projector utilized is a SONY VPL-EW276 with a resolution of 1280 × 800; the CCD camera used is a Microvision MV-VEM 120SM with a resolution of 1280 × 960; the telecentric lenses is a BT-2396 with a valid field of view of 51.6 mm × 38.7 mm when the CCD size is $1/3''$. During the experiments, a flat board played an important role: firstly, it was used to detect the coarse coordinates of the zero-phase point; secondly, it was used to detect the actual coordinates of the zero-phase point; lastly, it was used to calibrate the OCFPP system. Note that axes of the projector and camera should be carefully adjusted to be as parallel as possible before the formal 3D measurement.

4.1. Detection of zero-phase point with the CRPCM

The application of the CRPCM consists of two steps: firstly, the coarse coordinates of the zero-phase point was detected with the CFM; then, the RPCM was applied to obtain the fine coordinates of the zero-phase point.

Figure 11 depicts one of circular fringe patterns captured from a flat board, and its absolute phase. Three curves are plotted in figure 11(b). Each curve denotes pixels with the same phase value. They look like a set of arcs. Circle fitting was applied to them. The calculated centers are listed in table 1.

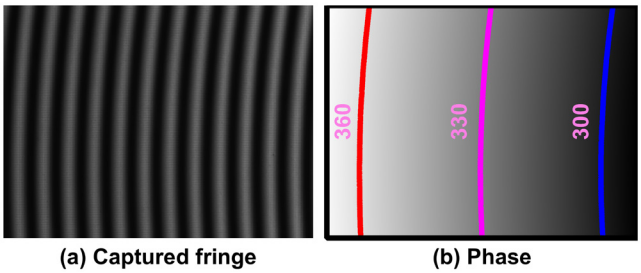

Figure 11. (a) A circular fringe pattern captured from a flat board, and (b) its phase: curves in (b) marks pixels with phase values of 360, 330, and 300 radians respectively.

Table 1. Zero-phase points detected with CFM.

Phase	300	330	360
Zero-phase point	(5930.4, 692.4)	(5929.0, 691.1)	(5946.2, 693.2)

Their average, $(5935, 692)$, was used as (x^c_{c0}, y^c_{c0}) in RPCM. To preliminarily check the validity of the searching center detected with CFP, 2DRM in [37] was also implemented. The result calculated with 2DRM is $(6069.16, 675.56)$. The two detected points are not far away. This is one piece of evidence that the CFM can provide a reasonable searching center. The actual performance of the CFM depends on the actual hardware layout accuracy and the phase accuracy.

Then RPCM was applied to detect the fine coordinates of the zero-phase point. During this process, configurations in figure 12 rather than those described in section 3.2 were adopted. This is to enhance the robustness of the searching process because noise is always unavoidable. Under these configurations, in total 694 times of plane fitting were adopted to obtain the coordinates of the zero-phase point with accuracy better than 0.05. The result is $(x_{c0}, y_{c0}) = (6004.31, 691.88)$. It can be found that coordinates of the zero-phase point calculated with RPCM, $(6004.31, 691.88)$, is not far from the one calculated with CFM, $(5935, 692)$. This is another piece of evidence that the CFM is capable of providing a reasonable searching center for the RPCM. It can also be found that the searching center provided by the CFM was more accurate than the one by the 2DRM in this experiment even though the 2D ruler is avoided. To validate the robustness of the RPCM, $(x^c_{c0}, y^c_{c0}) = (5935 + 100, 692 + 100)$ and $(x^c_{c0}, y^c_{c0}) = (5935 - 100, 692 - 100)$ were also tried. The results were also $(x_{c0}, y_{c0}) = (6004.31, 691.88)$. Therefore, the RPCM is robust in detecting the zero-phase point. If the PCM proposed in [37] is used to obtain coordinates of the zero-phase point with the same accuracy, the number of plane fitting required is $(1024/0.05 + 1) \times (1024/0.05 + 1) \approx 4.2 \times 10^8$. This is too time-consuming. The RPCM makes the efficiency of detecting the zero-phase point increased by about 6×10^5 times without loss of accuracy in this experiment.

4.2. 3D measurement of standard balls

Two standard balls were measured to further validate the proposed method. The diameters of them are 50.8035 mm and

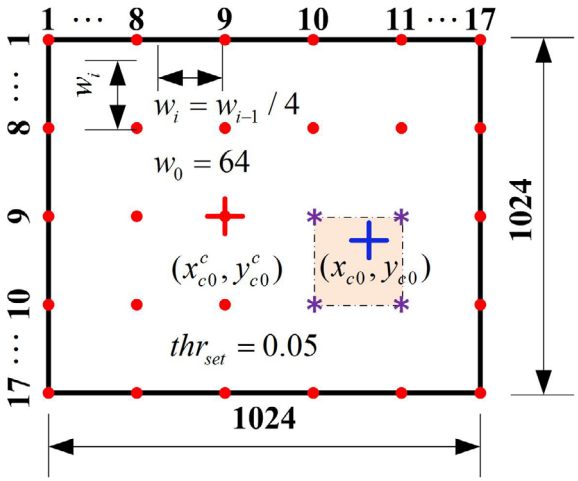

Figure 12. The searching strategy of the RPCM adopted in the experiments: the red cross whose coordinates are $(x^c_{c0}, y^c_{c0}) = (5935, 692)$ marks the center of the selected searching window, the first-round window size is 1024×1024, the first-round searching width is $w_0 = 64$, $\varepsilon = 4$, and $thr_{\text{set}} = 0.05$, the orange region signifies the region that covers the actual zero-phase point detected by one round of searching, the blue cross whose coordinates are (x_{c0}, y_{c0}) marks the actual zero-phase point, the purple asterisk denotes the points with the smallest $curvature(q)$ during the first-round search.

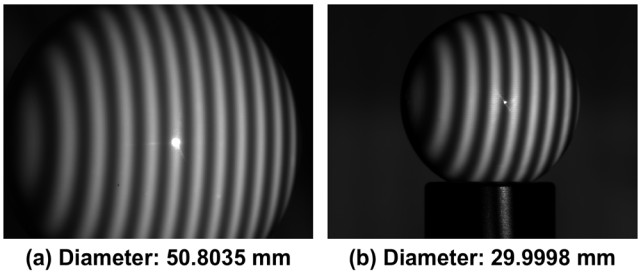

Figure 13. Circular fringe patterns captured from two standard balls during the experiment.

29.9998 mm respectively. Figure 13 shows the circular fringe patterns captured from these two standard balls. It can be found that there is a small part of saturated regions in both of the captured fringe patterns. This is because these standard balls are made of ceramic, and their surfaces are very smooth. In the following data processing, data in these saturated regions were discarded.

The 3D profiles of these two standard balls were recovered with the aid of zero-phase points detected with the CFM and CRPCM respectively. Figure 14 depicts the 3D profiles recovered with the CRPCM. Then sphere fitting was applied to the recovered profiles. Tables 2 and 3 list the results. In these tables, D signifies the fitted diameter, e_D signifies the difference between the fitted diameter and the actual diameter, and SD signifies the stand deviation of the sphere fitting. It can be found that the measurement accuracy when the CRPCM is used is better than that when the CFM is used. This is because the CRPCM is capable of detecting more accurate coordinates of the zero-phase point. However, the 3D measurement accuracy when the CFM is used is not too bad.

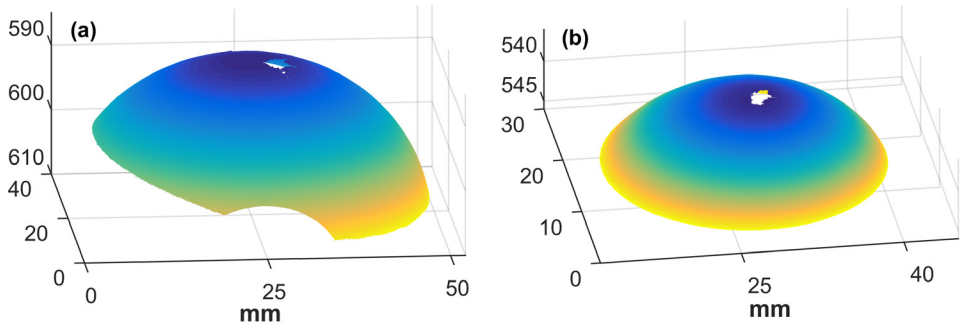

Figure 14. 3D profiles of the standard balls recovered with CRPCM whose diameters are (a) 50.8035 mm and (b) 29.9998 mm respectively.

Table 2. Results of sphere fitting applied to measured 3D data of the standard ball with diameter being 50.8035 mm (in millimeters).

Method	CFM	CRPCM
D	50.581	50.859
e_D	−0.222	0.056
SD	0.178	0.117

Table 3. Results of sphere fitting applied to measured 3D data of the standard ball with diameter being 29.9998 mm (in millimeters).

Method	CFM	CRPCM
D	30.107	30.035
e_D	0.107	0.035
SD	0.153	0.118

This further indicates that the zero-phase point detected with the CFM near its actual location.

SD is still not low enough even when the zero-phase point is detected with the CRPCM. This is not resulted by the CRPCM but by the accuracy of the calculated phase. As noted in [35], the phase accuracy of OCFPP is experimentally detected to be less than 1/7 of that of the conventional FPP. It can be improved to the same level as that of FPP by refining the hardware configuration which has not been accomplished at present.

Furthermore, it was found that obvious overall intensity variation among the captured circular fringe patterns might occur. This will bring damage to the 3D measurement accuracy. In our first experiment, this phenomenon arose when measuring the ball in figure 13(b). We re-conducted measurement to this ball, and the huge intensity variation disappeared. The intensity variation seems to be random. However, this phenomenon is not related to the proposed method. It will be further researched and analyzed in the future work.

4.3. Measurement of representative objects

Lastly, a mechanical part was measured with the CRPCM (see figure 15). This is just to demonstrate the effectiveness of the CRPCM in a more vivid way. Hence, no quantitative analysis will be given. Figure 16 shows the recovered profile. It is clear that the 3D profile of the mechanical part is well recovered.

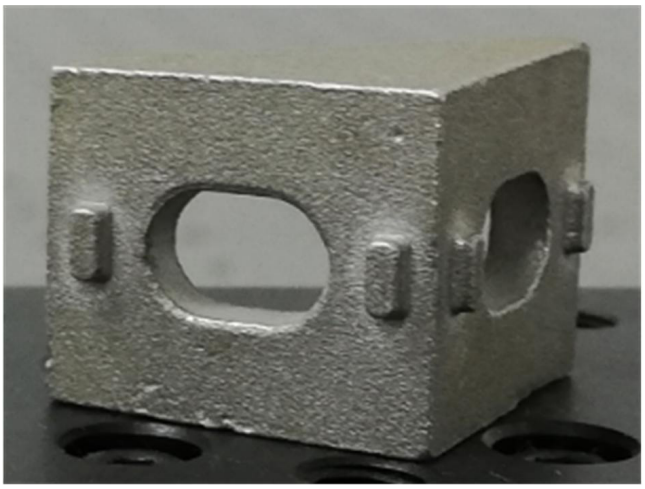

Figure 15. Image of a measured mechanical part.

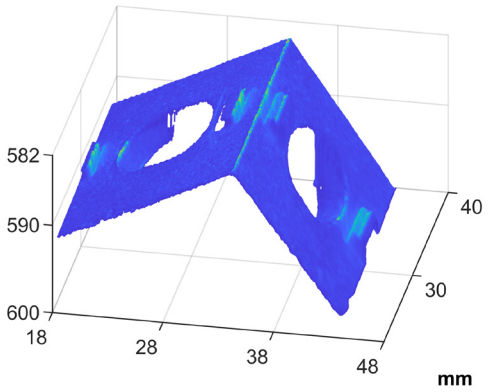

Figure 16. Recovered 3D profile of the measured mechanical part.

This indirectly demonstrates that the CRPCM works well in detecting the zero-phase point.

5. Conclusion

In this paper, the CRPCM is proposed to make it possible to detect the zero-phase point with both accuracy and efficiency for OCFPP. The CRPCM is composed of two related methods, the CFM and RPCM. The CFM is capable of finding the coarse location of the zero-phase point. It works by applying circle fitting to the phase of a circular fringe pattern captured from a flat board. The CFM provides the

searching center for the first-round search of RPCM. It helps to decrease the size of the searching window because the location it provides should be not far away from the actual location. RPCM is a modification of the PCM proposed in [37]. The main improvement lies in that a fast searching strategy is adopted in the RPCM to evidently decrease the time consumption. Mathematical deduction in combination with computer simulation is implemented to demonstrate the foundation of the fast searching strategy. The validity of the CRPCM is further demonstrated by a set of experiments. The CRPCM makes it possible to find the coarse location of the zero-phase point while getting rid of a 2D ruler, and dramatically raise efficiency of detecting the zero-phase point. The experiment shows that the efficiency of the CRPCM can be 6×10^5 times faster than that of the PCM.

Note that ideally the CRPCM is capable of accurately detecting coordinates of the zero-phase point, and the accuracy is only determined by the value of thr_{set} in equation (19); in practice, its accuracy relies on the phase accuracy, the accuracy of the hardware arrangement, and the planeness of the adopted flat board, etc.

Acknowledgments

The work in this paper was funded by the National Natural Science Foundation of China (NSFC) (Grant Nos. 61905190, 61975161, 61575157), the Natural Science Foundation of Jiangsu Province (Grant No. BK20190219), the Research Project of State Key Laboratory of Mechanical System and Vibration (Grant No. MSV201912), the China Postdoctoral Science Foundation (Grant No. 2018M633500), and the Natural Science Foundation of Shaanxi Province (Grant No. 2018JQ6063). Special thanks are given to Hehui Geng for assistance in drawing figure 5.

ORCID iDs

Chunwei Zhang https://orcid.org/0000-0002-1219-0791
Hong Zhao https://orcid.org/0000-0003-0927-8634

References

[1] Salvi J, Fernandez S, Pribanic T and Llado X 2010 A state of the art in structured light patterns for surface profilometry *Pattern Recognit.* **43** 2666–80
[2] Gorthi S S and Rastogi P 2010 Fringe projection techniques: whither we are? *Opt. Lasers Eng.* **48** 133–40
[3] Lohry W and Zhang S 2014 High-speed absolute three-dimensional shape measurement using three binary dithered patterns *Opt. Express* **22** 26752–62
[4] Pösch A, Schlobohm J, Matthias S and Reithmeier E 2017 Rigid and flexible endoscopes for three dimensional measurement of inside machine parts using fringe projection *Opt. Lasers Eng.* **89** 178–83
[5] Zuo C, Tao T, Feng S, Huang L, Asundi A and Chen Q 2018 Micro Fourier transform profilometry (μFTP): 3D shape measurement at 10 000 frames per second *Opt. Lasers Eng.* **102** 70–91
[6] Ren H, Li J and Gao X 2018 3D shape measurement of rail achieved by a novel phase measurement profilometry based on virtual reference fringe generated by image interpolation *Optik* **161** 348–59
[7] Beermann R, Quentin L, Reithmeier E and Kästner M 2018 Fringe projection system for high-temperature workpieces–design, calibration, and measurement *Appl. Opt.* **57** 4075–89
[8] Sicardi S A, Estrada J C, Martínez G A and Garnica G 2015 On axis fringe projection: a new method for shape measurement *Opt. Lasers Eng.* **69** 29–34
[9] Ma Y, Yin D, Wei C, Feng S, Ma J, Nie S and Yuan C 2019 Real-time 3D shape measurement based on radial spatial carrier phase shifting from circular fringe pattern *Opt. Commun.* **450** 6–13
[10] Takeda M and Mutoh K 1983 Fourier transform profilometry for the automatic measurement of 3D object shapes *Appl. Opt.* **22** 3977–82
[11] Qian K 2007 Two-dimensional windowed Fourier transform for fringe pattern analysis: principles, applications and implementations *Opt. Lasers Eng.* **45** 304–17
[12] Srinivasan V, Liu H C and Halioua M 1984 Automated phase-measuring profilometry of 3D diffuse objects *Appl. Opt.* **23** 3105–8
[13] Zhong J and Weng J 2005 Phase retrieval of optical fringe patterns from the ridge of a wavelet transform *Opt. Lett.* **30** 2560–2
[14] Takeda M 1996 Recent progress in phase-unwrapping techniques *Proc. SPIE* **2782** 334–44
[15] Zhao M, Huang L, Zhang Q, Su X, Asundi A and Qian K 2011 Quality-guided phase unwrapping technique: comparison of quality maps and guiding strategies *Appl. Opt.* **50** 6214–24
[16] Zhang C, Zhao H and Zhang L 2015 Fringe order error in multifrequency fringe projection phase unwrapping: reason and correction *Appl. Opt.* **54** 9390–9
[17] Zhang C, Zhao H and Jiang K 2016 Fringe-period selection for a multifrequency fringe-projection phase unwrapping method *Meas. Sci. Technol.* **27** 085204
[18] Zhang S 2018 Absolute phase retrieval methods for digital fringe projection profilometry: a review *Opt. Lasers Eng.* **107** 28–37
[19] Srinivasan V, Liu H C and Halioua M 1985 Automated phase-measuring profilometry: a phase mapping approach *Appl. Opt.* **24** 185–8
[20] Liu H, Su W, Reichard K and Yin S 2003 Calibration-based phase-shifting projected fringe profilometry for accurate absolute 3D surface profile measurement *Opt. Commun.* **216** 65–80
[21] Guo H, He H, Yu Y and Chen M 2005 Least-squares calibration method for fringe projection profilometry *Opt. Eng.* **44** 033603
[22] Zhang S and Huang P S 2006 Novel method for structured light system calibration *Opt. Eng.* **45** 083601
[23] Vo M, Wang Z, Hoang T and Nguyen D 2010 Flexible calibration technique for fringe-projection-based three-dimensional imaging *Opt. Lett.* **35** 3192–4
[24] Zhong K, Li Z, Li R, Shi Y and Wang C 2016 Pre-calibration-free 3D shape measurement method based on fringe projection *Opt. Express* **24** 14196–207
[25] Deetjen M E and Lentink D 2018 Automated calibration of multi-camera-projector structured light systems for volumetric high-speed 3D surface reconstructions *Opt. Express* **26** 33278–304
[26] Haskamp K, Kästner M and Reithmeier E 2011 Accurate calibration of a fringe projection system by considering telecentricity *Proc. SPIE* **8082** 80821B
[27] Chen Z, Liao H and Zhang X 2014 Telecentric stereo micro-vision system: calibration method and experiments *Opt. Lasers Eng.* **57** 82–92

[28] Li D, Liu C and Tian J 2014 Telecentric 3D profilometry based on phase-shifting fringe projection *Opt. Express* **22** 31826–35
[29] Yin Y, Wang M, Gao B Z, Liu X and Peng X 2015 Fringe projection 3D microscopy with the general imaging model *Opt. Express* **23** 6846–57
[30] Jeught S V D, Soons J A M and Dirckx J J J 2015 Real-time microscopic phase-shifting profilometry *Appl. Opt.* **54** 4953–9
[31] Rao L, Da F, Kong W and Huang H 2016 Flexible calibration method for telecentric fringe projection profilometry systems *Opt. Express* **24** 1222–37
[32] Li B and Zhang S 2017 Microscopic structured light 3D profilometry: binary defocusing technique versus sinusoidal fringe projection *Opt. Lasers Eng.* **96** 117–23
[33] Wang M, Yin Y, Deng D, Meng X, Liu X and Peng X 2017 Improved performance of multi-view fringe projection 3D microscopy *Opt. Express* **25** 19408–21
[34] Liu H, Lin H and Yao L 2017 Calibration method for projector-camera-based telecentric fringe projection profilometry system *Opt. Express* **25** 31492–508
[35] Zhao H, Zhang C, Zhou C, Jiang K and Fang M 2016 Circular fringe projection profilometry *Opt. Lett.* **41** 4951–4
[36] Zhao H, Zhang C, Zhou C, Jiang K and Fang M 2017 Circular fringe projection profilometry: erratum *Opt. Lett.* **42** 370
[37] Zhang C, Zhao H, Qiao J, Zhou C, Zhang L, Hu G and Geng H 2019 Three-dimensional measurement based on optimized circular fringe projection technique *Opt. Express* **27** 2465–77